An Indirect Matrix Converter for CCHP Microturbines in Data Center Power Systems

Andres Escobar
Department of Electrical Engineering
University of Arkansas
Fayetteville, AR, USA
axe011@uark.edu

Juan C. Balda
Department of Electrical Engineering
University of Arkansas
Fayetteville, AR, USA
jbalda@uark.edu

Claudio A. Busada
Departamento de Ingeniería Eléctrica y de Computadores,
Universidad Nacional del Sur
Bahía Blanca, Argentina
cbusada@uns.edu.ar

Dustin Christal
Department of Electrical Engineering
University of Arkansas
Fayetteville, AR, USA
dchrista@uark.edu

***Abstract* – Data centers (DCs) are considered critical loads that require premium power from utilities to ensure reliability at all times. Microturbine (MT) generation systems are becoming important in DCs, not only as distributed generation (DG) for supplying electricity, but also for providing cooling and heating functions, which is known as combined cooling, heat and power (CCHP) or tri-generation.**

This paper considers the use of an indirect matrix converter (IMC) as the power electronic interface (PEI) to connect a permanent magnet synchronous generator (PMSG) with the power grid in a DC. First, the paper analyzes the semiconductor losses for the IMC and the conventional back-to-back converter (BBC) as a function of the switching frequency in order to determine the favorable operating conditions for the IMC. It then presents a new control strategy that does not require measuring the grid voltages to inject the commanded power into the grid at unity power factor. Simulation results of a 15-kVA, 480-Vrms IMC-based MT generation system show the effectiveness of the proposed control technique for this particular application.

Keywords* – *Current control, data centers, distributed generation, indirect matrix converters, microturbines, permanent magnet synchronous generators

I. INTRODUCTION

Data centers are computational centers storing large amounts of information and equipment securely. They run efficiently and provide secure access to applications for users such as social network enterprises, government, financial institutions, news media, universities, etc. To operate without any interruptions, DCs require large amounts of premium power to ensure reliability [1], [2]. Thus, most DC installations have backup power generation systems (i.e., on-site generation and batteries) to provide redundancy when the main power supply fails. Besides electric power, information technology (IT) equipment requires proper cooling to prevent over-heating which may lead to early failures. The cooling system operates continuously and represents a major power consumer in DCs [3]–[5].

Microturbine units are used to drive high-speed PMSG and are becoming more attractive for on-site generation, in particular for loads under 5 MW that also require cooling and heating [6]. In a CCHP process, the wasted heat, a bi-product of the generating process, is used to produce the necessary cooling required by various pieces of equipment to operate safely, and thus, to improve system efficiency. MT-generator sets use different types of fuels to generate electricity (e.g., natural gas), their power range varies from 15 kW up to 1 MW, and operate at high speeds (e.g., 50,000~120,000 rpm). High rotational speeds produce high-frequency voltages that require an ac-ac converter to reduce the generator frequency to the grid frequency [7]. Many reasons are influencing the use of CCHP in DCs: efficiency increases, fossil-fuel energy consumption reductions, distribution line loading reductions, ability to produce cooling using an absorption chiller [6], [8], demand-side management capabilities, and reductions of CO_2 emissions into the atmosphere by a factor of 2 [9]. Fig. 1 shows a typical power distribution system for a DC that uses CCHP.

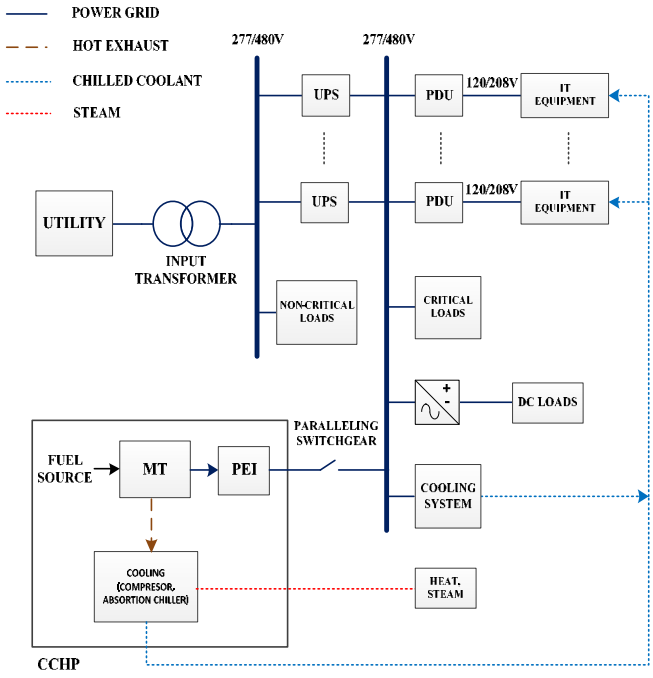

Fig. 1. Power distribution system for a DC with CCHP [3], [6]

978-1-4673-1000-0/12/$31.00 ©2012 IEEE

1.3

Conventionally, a BBC is used as the PEI to connect the high-frequency voltages generated by a PMSG driven by the MT with the power grid. The BBC consists of two stages that are connected via a dc link having electrolytic capacitors which are well known for their reduced lifetime [10], limiting the BBC mean time between failures. These capacitors are bulky, heavy and unreliable, so they are considered one of the main failure causes in BBCs [11]. Furthermore, grid-connected applications require synchronizing the generator with the grid using a phase-locked loop (PLL) algorithm sensing the grid voltages [12], [13]. The PLL algorithm produces the magnitude, phase and frequency of the grid voltages to synchronize the generator.

In the last two decades, the IMC has been widely analyzed as adjustable-speed drives for motor applications; however, some disadvantages such as the low input/output voltage ratio limited to 86%, the complexity of the control techniques to guarantee proper waveforms and safe operation, and the lack of ride-through capabilities have kept the IMC from being adopted by industry [14]–[19]. Despite these disadvantages, IMC may be an alternative for particular applications [18], [19] such as low power, low voltage/fixed frequency ac-to-ac generation where it is possible to adjust the output voltage of a generator to meet grid voltage requirements. Indirect matrix converters have been proposed as a PEI to connect a variable-speed PMSG with a load operating at grid frequency [20]–[22]. The IMC does not have bulky and lifetime-limited dc-link electrolytic capacitors [14], [18]; thus, the converter life span can be improved while facilitating a compact PEI.

Taking into account the above, the paper presents first an analysis of the semiconductor losses in both the IMC and BBC to identify those operating conditions which are more favorable to the IMC. The paper then develops a new control strategy for the inverter stage of the IMC that does not require sensing the grid voltages to connect the IMC inverter stage with the grid. Instead, the IMC output currents, decomposed in the $d-q$ synchronous frame, are used to calculate the inverter output voltages.

This paper is divided into the following sections: Section II presents the implementation of an IMC as a PEI for a DC, and compares the BBC and the IMC in terms of efficiency. Section III provides an introduction to the space vector modulation (SVM) control technique used to control the IMC inverter and rectifier. Section IV presents the proposed new control strategy for the IMC inverter to regulate the injected currents. Lastly, Section V analyzes results from simulations to demonstrate the capability of the IMC to connect a high-frequency generating unit with the power grid.

II. INDIRECT MATRIX CONVERTER AS A PEI FOR DCS

Figure 2 depicts a DG system based on a MT that uses an IMC as a PEI. For simplicity, the PMSG is modeled as ideal three-phase voltage sources in series with synchronous inductances, and filters are placed at the input and output of the IMC to filter high-order harmonics that otherwise could affect the PMSG operation and the power quality delivered to

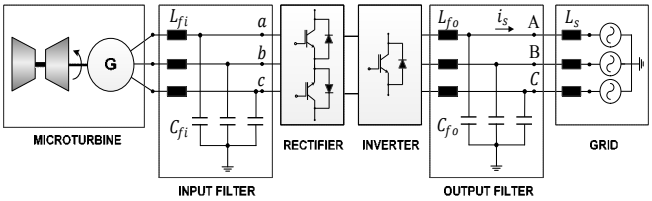

Fig. 2. IMC interfacing a high-frequency PMSG with the power grid

the load. In all cases, the total harmonic distortions (THD) for input currents and output voltages should be less than 5% [23]. The grid is also modeled as inductors in series with ideal three-phase voltage sources. The rectifier is made of IGBTs connected in back-to-back configuration to provide IMC bidirectional capability required during start up when the MT operates as a motor drawing power from the grid (motor mode). Once the MT speed threshold is reached, the MT injects power back into the grid (generator mode). The inverter has the same structure as a conventional inverter "brick".

A. IMC Loss Calculations

Converter loss calculations are very important to estimate the overall efficiency of the power converter, and to help sizing the cooling system required for the application. In general, the total semiconductor losses of the converters are calculated as the sum of conduction and switching losses. Conduction losses are predominant at low switching frequencies, and switching losses are more significant at high frequencies. The conduction losses are caused mainly by the on-state resistance and on-state voltage across each switch or diode while conducting. The switching losses are due to the commutation process of the semiconductor device depending on the switching frequency as well as the turn-on and turn-off energies dissipated by each device [24].

As shown in Fig. 2, the IMC contains two bridges: the rectifier that is treated as a current source bridge (CSB) and the inverter treated as a voltage source bridge (VSB) [25].

For the rectifier, the conduction losses P_{c_CSB} are calculated as:

$$P_{c\_CSB} = \frac{9}{2\pi}(V_{CEo} + V_{Do})m_r I_o cos\varphi_o + \frac{3\sqrt{3}}{2\pi^2}(r_{CE} + r_D)m_r I_o^2(1 + 4cos^2\varphi_o) \quad (1)$$

where m_r is the rectifier modulation index, I_o the peak output current and φ_o the output angular displacement. No switching losses are present in this stage since it switches when a zero-voltage state is applied to the inverter [26].

For the inverter, the switching losses P_{sw_VSB} and the conduction losses P_{c_VSB} are calculated as follows:

$$P_{sw\_VSB} = \frac{27}{\pi^2} f_{sw}(E_{on} + E_{off} + E_{rr}) \frac{V_i}{V_{dcnom}} \frac{I_o}{I_{cnom}} cos\varphi_i \quad (2)$$

$$P_{c\_VSB} = 6\left[\frac{(V_{CEo}+V_{Do})I_o}{2\pi} + \frac{(V_{CEo}-V_{Do})I_o}{8} m_i cos\varphi_o + \frac{(r_{CE}+r_D)I_o^2}{8} + \frac{(r_{CE}-r_D)I_o^2}{3\pi} m_i cos\varphi_o\right] \quad (3)$$

where m_i is the inverter modulation index, V_i the peak input phase voltage, φ_i the input angular displacement and f_{sw} the switching frequency.

The methods described in [25]–[27] are used to calculate the losses for the IMC considering the discrete IKW40N120H3 IGBTs from Infineon. Table I lists IGBT and diode parameters. Figure 3 shows the BBC and IMC efficiencies for switching frequencies up to 40 kHz and output currents from 0 A to 30 A. The IMC becomes more efficient for switching frequencies higher than 10 kHz; this is mainly caused due to the capability of commutating the IMC rectifier during the zero-current periods of the dc link (zero-voltage vector applied to the inverter), which reduces rectifier switching losses.

TABLE I. Semiconductor Device Parameters

Parameter	Symbol	Nominal value
IGBT zero-current voltage drop	V_{CEo}	1.05 V
IGBT on-state resistance	r_{CE}	25 mΩ
IGBT conduction current under nominal conditions	I_{cnom}	40 A
IGBT dc-bus voltage under nominal conditions	V_{dcnom}	600 V
IGBT turn-on switching loss under nominal conditions	E_{on}	3.20 mJ
IGBT turn-off switching loss under nominal conditions	E_{off}	1.20 mJ
Diode zero-current forward voltage drop	V_{Do}	1.65 V
Diode on-state forward resistance	r_D	22 mΩ

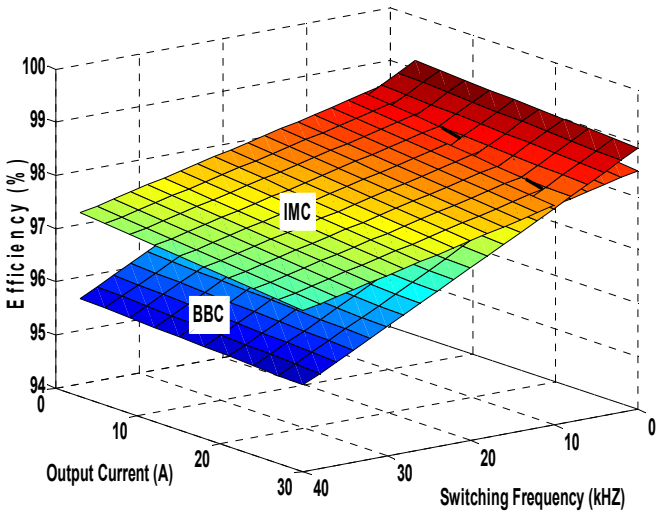

Fig. 3. Comparison between BBC and IMC calculated efficiencies based on a 15-kVA converter at 480-Vrms output voltage

The selection of the switching frequency is a trade-off between IMC passive components size and system efficiency, and has an impact on the electromagnetic interference (EMI) and THD [28]. When the f_{sw} changes from 20 kHz to 30 kHz there is a 50% reduction in the value of the input inductance L_{fi} (assuming C_{fi} equals to 50 μF for both cases). Based on this result, the switching frequency f_{sw} for the proposed PEI using an IMC is selected to be 30 kHz since it is beyond the audible noise range and the calculated converter efficiency is above 96%.

III. INDIRECT MATRIX CONVERTER CONTROL STRATEGY

To control the IMC rectifier and inverter, a SVM control technique has been traditionally proposed to produce the desired input/output current/voltage sinusoidal waveforms [29]. The duty cycles in each stage are synchronized in order to provide safe commutation for the rectifier; i.e., rectifier commutates when a null vector is applied to the inverter.

A. Rectifier Stage

It is well known that there are 8 possible combinations for the rectifier switches: 6 active or non-zero vectors; so the desired IMC input currents can be synthesized by making use of the two adjacent active vectors defining any of the SVM six sectors to realize the commanded current vector I_{in} [30].

Fig. 4(a) depicts the current vector I_{in} in sector I. The duty cycles d_α^r, d_β^r and d_o^r that are used to synthesize this vector are calculated as follows [29]:

$$\begin{aligned} d_\alpha^r &= m_r \sin(\pi/3 - \theta_{in}) \\ d_\beta^r &= m_r \sin(\theta_{in}) \\ d_o^r &= 1 - d_\alpha^r - d_\beta^r \end{aligned} \quad (4)$$

where θ_{in} is the reference current angle with respect to the considered sector. The IMC input currents can be represented as:

$$\begin{bmatrix} i_a \\ i_b \\ i_c \end{bmatrix} = \begin{bmatrix} d_\alpha^r + d_\beta^r \\ -d_\alpha^r \\ -d_\beta^r \end{bmatrix} I_{dc,} \quad (5)$$

and taking into account that $\theta_{in} = (\omega_i t - \varphi_i + \pi/6)$ yields

$$\begin{bmatrix} i_a \\ i_b \\ i_c \end{bmatrix} = m_r \begin{bmatrix} \cos(\omega_i t - \varphi_i) \\ \cos(\omega_i t - \varphi_i - 2\pi/3) \\ \cos(\omega_i t - \varphi_i + 2\pi/3) \end{bmatrix} I_{dc} \quad (6)$$

with $0 \le m_r = I_{in}/I_{dc} \le 1$ and ω_i the input angular frequency. Thus, the input currents can be represented as:

$$\begin{bmatrix} i_a \\ i_b \\ i_c \end{bmatrix} = I_{in} \begin{bmatrix} \cos(\omega_i t - \varphi_i) \\ \cos(\omega_i t - \varphi_i - 2\pi/3) \\ \cos(\omega_i t - \varphi_i + 2\pi/3) \end{bmatrix} \quad (7)$$

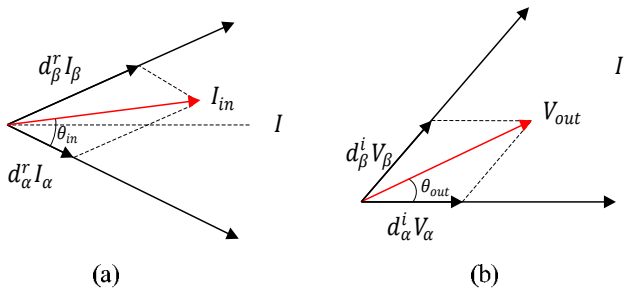

Fig. 4. Rectifier (a) and inverter (b) space vector diagram in sector I [29]

B. *Inverter Stage*

The inverter stage must always switch in such a manner that provides a path for the current; otherwise, the semiconductor devices could be destroyed due to undesired overvoltages [30]. In this stage, there are also 6 possible combinations that produce non-zero output voltages and 2 combinations that produce a zero or null output voltage. Likewise for the rectifier stage, the desired output voltage can be determined by using the duty cycles d_α^i, d_β^i and d_o^i in any considered sector [29].

For sector I,

$$\begin{aligned} d_\alpha^i &= m_i \sin\left({}^{\pi}/_{3} - \theta_{out}\right) \\ d_\beta^i &= m_i \sin(\theta_{out}) \\ d_o^i &= 1 - d_\alpha^i - d_\beta^i \end{aligned} \tag{8}$$

where θ_{out} is the reference voltage angle with respect to this sector. As presented in Fig 4(b), the line-to-line voltages can be written as follows:

$$\begin{bmatrix} v_{AB} \\ v_{BC} \\ v_{CA} \end{bmatrix} = \begin{bmatrix} d_\alpha^i + d_\beta^i \\ -d_\alpha^i \\ -d_\beta^i \end{bmatrix} V_{dc,ave} \tag{9}$$

For sector I, $\theta_{out} = \left(\omega_o t - \varphi_o + {}^{\pi}/_{3}\right)$ then,

$$\begin{bmatrix} v_{AB} \\ v_{BC} \\ v_{CA} \end{bmatrix} = m_i \begin{bmatrix} \cos\left(\omega_o t - \varphi_o + {}^{\pi}/_{6}\right) \\ \cos\left(\omega_o t - \varphi_o + {}^{\pi}/_{6} - {}^{2\pi}/_{3}\right) \\ \cos\left(\omega_o t - \varphi_o + {}^{\pi}/_{6} + {}^{2\pi}/_{3}\right) \end{bmatrix} V_{dc,ave} \tag{10}$$

with $0 \le m_i = \sqrt{3} V_{out} / V_{dc,ave} \le 1$, $V_{dc,ave}$ the average dc-link voltage [31] and ω_o the output angular frequency. Then, the output line-to-line voltages can be represented as:

$$\begin{bmatrix} v_{AB} \\ v_{BC} \\ v_{CA} \end{bmatrix} = \sqrt{3} V_{out} \begin{bmatrix} \cos\left(\omega_o t - \varphi_o + {}^{\pi}/_{6}\right) \\ \cos\left(\omega_o t - \varphi_o + {}^{\pi}/_{6} - {}^{2\pi}/_{3}\right) \\ \cos\left(\omega_o t - \varphi_o + {}^{\pi}/_{6} + {}^{2\pi}/_{3}\right) \end{bmatrix} \tag{11}$$

IV. Proposed Control Strategy for the IMC

Applying Kirchhoff's voltage law to the equivalent per-phase circuit of the three phase inverter of the IMC and the grid, the voltages in the $d-q$ frame can be written as:

$$p i_s^{dq} = \frac{1}{L_s}\left(v_{inv}^{dq} - v_s^{dq} - j\omega_o L_s i_s^{dq}\right) \tag{12}$$

where vectors like $v_s^{dq} = v_s^d + j v_s^q$ are constant and rotate at the inverter synchronous speed (i.e., the grid frequency) under steady-state conditions. It is observed that the current is dependent on the cross-coupling terms $\omega_o L_s i_s^d$ and $\omega_o L_s i_s^q$. Eliminating this cross-coupling through the control algorithm should improve the system response.

Conventionally, the voltage oriented control technique (VOC) is used to regulate the active and reactive currents injected by the inverter [32], [33]. For this technique, it is required to sense the grid voltages to determine the required inverter output voltages. To avoid sensing the grid voltages and decoupling the dynamics of the $d-q$ axes, the following control technique is proposed:

$$v_{inv}^{dq} = -\frac{p\tau + 1}{pC + g} i_s^{dq} + j\omega_o L_s i_s^{dq} \tag{13}$$

where p represents the derivative operator, C the forward indirect gain, τ the forward direct gain, and g is the conductance gain used to determine the currents injected into the grid at unity displacement power factor and resulting from higher-level controller not shown here [34].

The feed-forward terms $j\omega_o L_s i_s^{dq}$ are used to decouple the cross-coupling terms, and thus, to improve the dynamic response of the system. Substituting (13) into (12) yields,

$$p i_s^{dq} = \frac{1}{L_s}\left(-\frac{p\tau + 1}{pC + g} i_s^{dq} - v_s^{dq}\right), \tag{14}$$

and,

$$i_s^{dq} = -\frac{pC + g}{p^2 L_s C + (L_s g + \tau)p + 1} v_s^{dq} \tag{15}$$

If the transfer function in (15) is stable, then, under steady-state conditions ($p \to 0$):

$$i_s^{dq} = -g v_s^{dq} \tag{16}$$

From (16), the currents are in phase with the grid voltages. If the conductance g is positive, the inverter draws power from the grid; and if negative, the inverter injects power into the grid. The schematic of the proposed control strategy is presented in Fig. 5.

V. Simulations Results

In order to determine the feasibility of the proposed controller, the MT-PMSG system whose parameters are listed in Table II and topology given in Fig. 2 was implemented in Matlab/Simulink™. For this case, IGBTs are ideal switches, m_r is set to 1 to provide the maximum IMC voltage transfer ratio, and the PMSG output voltage is set to 640 Vrms to overcome a 10% voltage drop in the IMC filters and the 86% IMC voltage ratio limitation. Input and output filters are sized in order to get a THD lower than 5% in the input current and the output voltage [23], and have cut-off frequencies of 4 kHz and 1 kHz, respectively. The gains τ and C, are selected to make the denominator of (15) stable.

TABLE II. Parameters of the MT-PMSG System

Parameter	Nominal value
IMC rated power	15 kVA
Generator line-to-line voltage	640 Vrms
Generator frequency	400 Hz
Grid line-to-line voltage	480±5% Vrms
Grid equivalent impedance	L_s=3 mH
Grid frequency	60 Hz
LC input filter	L_{fi}=50 µH, C_{fi}=50 µF
LC output filter	L_{fo}=3 mH, C_{fo}=5 µF
Switching frequency	30 kHz
C	0.0003 $s\Omega^{-1}$
τ	0.002 s

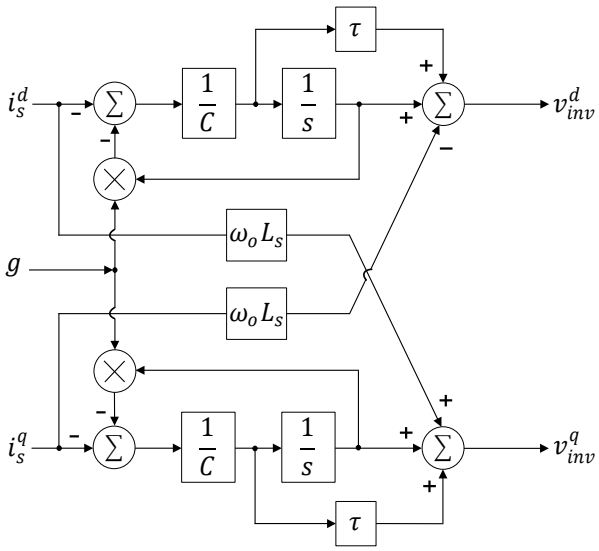

Fig. 5. Proposed control block diagram for the IMC inverter

Fig. 6 shows the i_d current variation (red) when the reference current (black) changes while i_q (blue) remains relatively unchanged since unity power factor is commanded. It is desired to inject 8 Arms at $t = 20\,ms$ ($g = \frac{8}{277} = 0.028$ Ʊ), and 13 Arms at $t = 50\,ms$ ($g = \frac{13}{277} = 0.047$ Ʊ). The d-axis current follows the reference which is a (negative) replica of the conductance g. The settling time is under 10 ms with a 23% overshoot for the worst case. By changing the forward direct and indirect gains in the stable region, it is possible to decrease the settling time. However, this causes larger overshoots in the current. As shown in Fig. 7, the inverter output line-to line voltages are nearly sinusoidal with a THD_v of 3.54%. The 20% overshoot in only the voltage between phases a and b at $t = 20\,ms$ is a transient caused as the controller commands new switching states for the inverter in response to a change in the commanded currents; however, this transient does not affect the system stability or semiconductor devices. Lastly, Fig. 8. shows the three-phase currents injected into the grid with a 3.1% THD_i.

VI. CONCLUSIONS

This paper extended the body of knowledge related to using an IMC to connect a high-frequency MT-PMSG set to the power distribution system of a data center. An analysis of the semiconductor device losses showed that the IMC becomes more efficient than the BBC for switching frequencies above 10 kHz. This was mainly due to the capability of reducing rectifier switching losses by switching the IMC rectifier when the null voltage vector was applied to the inverter stage. The IMC high-frequency operation should allow for size reductions of the filter components, and thus, size reductions of the PEI required for the MT.

A new control strategy in the $d-q$ frame was presented to control the current injected by the IMC into the grid without sensing the grid voltages. Simulation results illustrated the feasibility of the control technique to inject the commanded currents without causing any significant or adverse overvoltages or overcurrents.

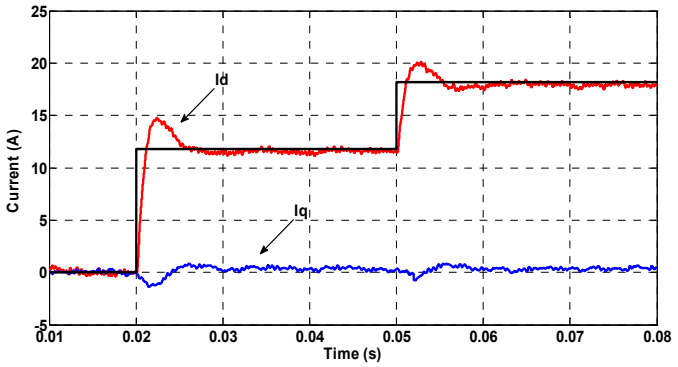

Fig. 6. d and q current variations for changes of the reference current

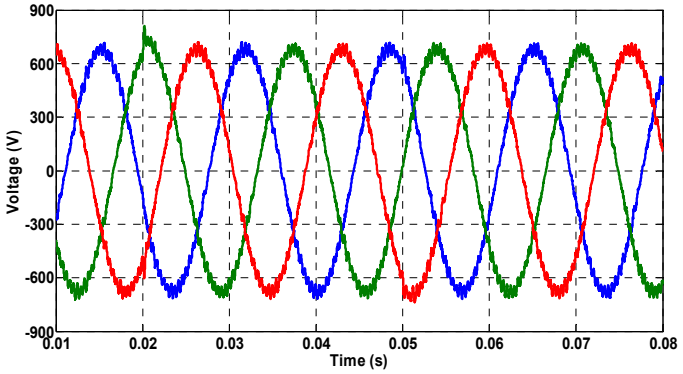

Fig. 7. Inverter output line voltage

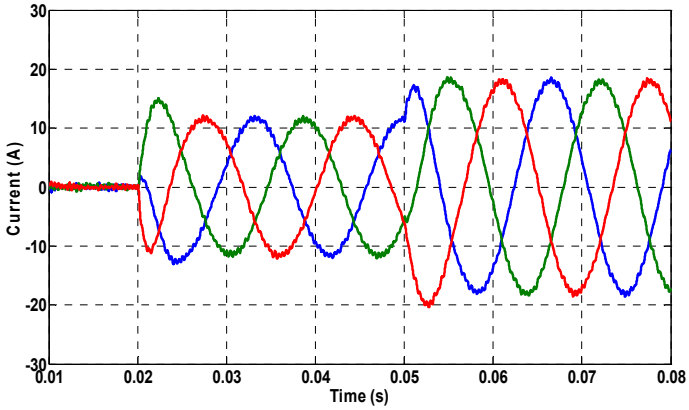

Fig. 8. Output currents of the IMC

VII. ACKNOWLEDGMENTS

The authors are grateful for the financial support from GRid-connected Advanced Power Electronics Systems (GRAPES), a National Science Foundation Industry/University Cooperative Research Center. Mr. Andrés Escobar Mejía is grateful for the financial support from the Fulbright Program and the Universidad Tecnológica de Pereira (Colombia).

VIII. REFERENCES

[1] S. Satish Rajagopalan, B. Fortenbery, D. Symanski, "Power quality disturbances within DC data centers," in *IEEE 32nd International Telecommunications Energy Conference*, pp. 1–7, June 2010.

[2] K.E. Herold, R. Radermacher, "Integrated power and cooling systems for data centers," in *Proceedings of the International Society on Thermal Phenomena*, pp. 808–811, August 2002.

[3] M. Seymour, C. Aldham, M. Warner, H. Moezzy, "The increasing challenge of data center design and management: Is CFD a must?," in *Electronics Cooling Magazine*, pp. 28–33, December 2011.

[4] U.S. Environmental Protection Agency ENERGY STAR Program, "Report to Congress on Server and Data Center Energy Efficiency Public Law 109-431, August 2007. [Online]. Available: http://www.energystar.gov/ia/partners/prod_development/downloads/EPA_Datacenter_Report_Congress_Final1.pdf

[5] National Renewable Energy Laboratory (NREL), Best practices guide for energy-efficient data center design," U.S. Department of Energy, March 2011. [Online]. Available: http://www1.eere.energy.gov/femp/pdfs/eedatacenterbestpractices.pdf

[6] K. Darrow, B. Hedman, "Opportunities for combined heat and power in data centers, ICF International, March 2009. [Online]. Available: http://www1.eere.energy.gov/manufacturing/datacenters/pdfs/chp_data_centers.pdf

[7] S. Grillo, S. Massucco, A. Morini, A. Pitto, F. Silvestro, "Microturbine control modeling to investigate the effects of distributed generation in electric energy networks," *IEEE Systems Journal*, vol. 4, no. 3, pp. 303–312, September 2010.

[8] EPA CHP Partnership, "Combined Heat and Power," [Online]. Available: http://www.epa.gov/chp/documents/datacenter_fs.pdf

[9] U.S. Environmental Protection Agency Combined Heat and Power Partnership, "The role of distributed generation and combined heat and power (CHP) systems in data centers," August 2007. [Online]. Available: http://www.epa.gov/chp/documents/datactr_whitepaper.pdf

[10] S. K. Maddula, J. C. Balda, "Lifetime of electrolytic capacitors in regenerative induction motor drives," in *Proceedings of the IEEE 36th Power Electronics Specialists Conference*, pp. 153–159, June 2005.

[11] R. Lai, F. Wang, R. Burgos, Y. Pei, D. Boroyevich, B. Wang, T.A. Lipo, V.D. Immanuel, K.J. Karimi, "A systematic topology evaluation methodology for high-density three-phase PWM AC-AC converters," *IEEE Transactions on Power Electronics*, vol. 23, no. 6, pp. 2665–2680, November 2008.

[12] S.-K, Chung, "Phase-locked loop for grid-connected three-phase power conversion systems," in *Proceedings of the IEE Electric Power Applications*, vol. 147, no. 3, vol. 147, pp. 213–219, May 2000.

[13] P. Rodríguez, A. Luna, I. Candela, R. Mujal, R. Teodorescu, F. Blaabjerg, "Multiresonant frequency-locked loop for grid synchronization of power converters under distorted grid conditions," *IEEE Transactions on Industrial Electronics*, vol. 58, no. 1, pp. 127–138, January 2011.

[14] N. Mahendran, G. Gurusamy, "Replacement of two step power conversion system using matrix converter," *European Journal of Scientific Research*, vol. 48, no. 2, pp. 238–248, 2010.

[15] P. W. Wheeler, J. Rodríguez, J. C. Clare, L. Empringham, A. Weinstein "Matrix Converters: A Technology Review," *IEEE Transactions on Industrial Electronics*, vol. 49, no. 2, pp. 276–288, April 2002.

[16] J.W. Kolar, T. Friedli, F. Krismer, S. D. Round, "The essence of three-phase AC/AC converter systems," in *Proceedings of EPE-PEMC*, pp. 27-42, September 2008.

[17] S. Bernet, S. Ponnaluri, R. Teichmann, "Design and loss comparison of matrix converters and voltage-source converters for modern AC drives," *IEEE Transactions on Industrial Electronics*, vol. 49, no. 2, pp. 304–314, April 2002.

[18] J.W. Kolar, F. Schafmeister, S. D. Round, H. Ertl, "Novel three-phase ac-ac sparse matrix converters," *IEEE Transaction on Power Electronics*, vol. 22, no. 5, pp. 1649–1661, September 2007.

[19] T. Friedli, J.W. Kolar, "Comprehensive comparison of three-phase ac-ac matrix converter and voltage dc-link back-to-back converter systems," in *Proceedings of IEEE/IEEJ International Power Electronics Conference,* IPEC 2010, Sapporo, Japan, pp. 2789-2798, June 21–24, 2010.

[20] J.A. Andrade-Romero, J.F. Romero, M. Rafikov, "Optimal control of indirect matrix converter based microturbine generation system," in *proceedings of the 9th International Conference in Control and Automation (ICCA)*, pp. 1085–1090, December 2011.

[21] M. Hamouda, K. All-Haddad, H. Blanchette, "Input-state feedback linearization control of two-stage matrix converters interfaced with high-speed microturbine generators," in *proceedings of the IEEE Canada Electrical power Conference,* pp. 302–307, October 2007.

[22] Wenlang, C. Zhiyoung, Y. Lingzhi, Y. Ning, "Modeling and control on grid-connected inverter stage of two-stage matrix converter for direct-drive wind power system," in *Proceedings of the 29th Chinese Control Conference,* pp. 4928–4932, July 2010.

[23] *IEEE Recommended practices and requirements for harmonic control in electrical power system*, IEEE Standard 519, June 1992.

[24] M. Apap, J.C. Clare, P.W. Wheeler, M. Bland, K. Bradley, "Comparison of losses in matrix converters and voltage source inverters," in *Proceedings of the IEE Seminar on Matrix Converters*, London, U.K., pp. 4/1–4/6, April 2003.

[25] B. Wang, G. Venkataramanan, "Analytical modeling of semiconductor losses in matrix converters," in *Proceedings of the CES/IEEE 5th International Power and Motion Control Conference, IPEMC 2006*, August 2006.

[26] S. Round, F. Schafmeister, M. Heldwein, E. Pereira, L. Serpa, J. Kolar, "Comparison of performance and realization effort of a very sparse matrix converter to a voltage DC link PWM inverter with active front end," *IEEJ Transaction*, vol. 126-D, no. 5, pp. 578–588, May 2006.

[27] D. Graovac, M. Pürschel, "IGBT power losses calculation using date-sheet parameters," Infineon, Application note, version 1.1, January 2009.

[28] M.L Heldwein, J.W. Kolar, "Impact of EMC filters on the power density of modern three-phase PWM converters," *IEEE Transactions on Power Electronics,* vol. 24, no. 6, pp. 1577–1588, June 2009.

[29] M.Y Lee, P. Wheeler, Christian Klumpner, "Space-Vector modulated multilevel matrix converter," *IEEE Transactions on Industrial electronics,* vol. 57, no. 10, pp. 3385–3394, October 2010.

[30] M. Hamouda, F. Fnaiech, K. Al-Haddad, "Space vector modulation scheme for dual-bridge matrix converters using safe-commutation strategy," in *Proceedings of the 31st Annual Conference of IEEE Industrial Electronics Society, IECON 2005*, pp. 1060–1065, November 2005.

[31] L. Huber, D. Borojević, "Space vector modulated three-phase to three-phase matrix converter with input power factor correction," *IEEE Transactions on Industry Applications*, vol. 31, no. 6, pp. 1234–1246, November/December 1995.

[32] R. Kadri, J.-P. Gaubert, G. Champenois, "An improved maximum power point tracking for photovoltaic grid-connected inverter based on voltage-oriented control," *IEEE Transactions on Industrial Electronics*, vol. 58, no. 1, pp. 66–75, January 2011.

[33] S.A. Larrinaga, M.A. Rodríguez, E. Oyarbide, J.R. Torrealday, "Predictive control strategy for DC/AC converters based on direct power Control," *IEEE Transactions on Industrial Electronics*, vol. 54, no. 3, pp. 1261–1271, June 2007.

[34] H. Nikkhajoei, M.R. Iravani, "A matrix converter based micro-turbine distributed generation system," *IEEE Transactions on Power Delivery*, vol. 20, no. 3, pp. 2182–2192, July 2005.